

Adaptive Terminal Guidance for Hypervelocity Impact in Specified Direction

Ping Lu*

Iowa State University, Ames, IA 50011-2271

David B. Doman†

Air Force Research Laboratory, WPAFB, OH 45433-7531

John D. Schierman‡

Barron Associates, Inc., Charlottesville, VA 22901

Abstract

The problem of guiding a hypersonic gliding vehicle in the terminal phase to a target location is considered. In addition to the constraints on its final position coordinates, the vehicle must also impact the target from a specified direction with very high precision. The proposed 3-dimensional guidance laws take simple proportional forms. The analysis establishes that with appropriately selected guidance parameters the 3-dimensional guided trajectory will satisfy these impact requirements. We provide the conditions for the initial on-line selection of the guidance law parameters for the given impact direction requirement. The vehicle dynamics are explicitly taken into account in the realization of guidance commands.

*Professor, Department of Aerospace Engineering, 2271 Howe Hall; plu@iastate.edu, Associate Fellow AIAA

†Senior Aerospace Engineer, 2210 Eighth Street, Bldg. 146, Room 305, David.Doman@wpafb.af.mil, Senior Member AIAA

‡Senior Research Scientist, Suite 202, 1410 Sachem Place, schierman@bainet.com, Associate Fellow AIAA

Report Documentation Page

Form Approved
OMB No. 0704-0188

Public reporting burden for the collection of information is estimated to average 1 hour per response, including the time for reviewing instructions, searching existing data sources, gathering and maintaining the data needed, and completing and reviewing the collection of information. Send comments regarding this burden estimate or any other aspect of this collection of information, including suggestions for reducing this burden, to Washington Headquarters Services, Directorate for Information Operations and Reports, 1215 Jefferson Davis Highway, Suite 1204, Arlington VA 22202-4302. Respondents should be aware that notwithstanding any other provision of law, no person shall be subject to a penalty for failing to comply with a collection of information if it does not display a currently valid OMB control number.

1. REPORT DATE 2006		2. REPORT TYPE		3. DATES COVERED 00-00-2006 to 00-00-2006	
4. TITLE AND SUBTITLE Adaptive Terminal Guidance for Hypervelocity Impact in Specified Direction				5a. CONTRACT NUMBER	
				5b. GRANT NUMBER	
				5c. PROGRAM ELEMENT NUMBER	
6. AUTHOR(S)				5d. PROJECT NUMBER	
				5e. TASK NUMBER	
				5f. WORK UNIT NUMBER	
7. PERFORMING ORGANIZATION NAME(S) AND ADDRESS(ES) Air Force Research Laboratory, Air Vehicles Directorate, Wright Patterson AFB, OH, 45433				8. PERFORMING ORGANIZATION REPORT NUMBER	
9. SPONSORING/MONITORING AGENCY NAME(S) AND ADDRESS(ES)				10. SPONSOR/MONITOR'S ACRONYM(S)	
				11. SPONSOR/MONITOR'S REPORT NUMBER(S)	
12. DISTRIBUTION/AVAILABILITY STATEMENT Approved for public release; distribution unlimited					
13. SUPPLEMENTARY NOTES					
14. ABSTRACT					
15. SUBJECT TERMS					
16. SECURITY CLASSIFICATION OF:			17. LIMITATION OF ABSTRACT	18. NUMBER OF PAGES 36	19a. NAME OF RESPONSIBLE PERSON
a. REPORT unclassified	b. ABSTRACT unclassified	c. THIS PAGE unclassified			

To ensure high accuracy in the impact angle conditions in an operational environment, we develop closed-loop nonlinear adaptation laws for the guidance parameters. We present the complete guidance logic and associated analysis. Simulation results are provided to demonstrate the effectiveness and accuracy of the proposed terminal guidance approach.

I. Introduction

Recent interests in developing on-demand global-reach payload delivery capability have brought to the forefront a number of underlying technological challenges. Such operations will involve responsive launch, autonomous entry flight, and precision terminal maneuvers. In certain scenarios the mission requirements call for the payload to impact the target location from a specific direction with supersonic speed. One example is to impact the target in a direction perpendicular to the tangent plane of the terrain at the target. The terminal guidance system will be responsible for directing the vehicle to the target and achieving the desired impact direction. The impact precision requirements under the scenarios considered are very high and stringent. For instance, the required Circular Error Probable (CEP) of the impact distance is just 3-meter.¹ The errors of the impact angles are desired to be within 0.5 deg. The very high speeds throughout the terminal phase only make it considerably more difficult to achieve these levels of precision. Yet cost considerations dictate that the terminal guidance algorithm should be relatively simple and computationally tractable for real-time operations.

While a number of guidance methods can guide the vehicle to the target, not many address the unique need for impact from a specific direction. One method that can is the so-called “dive-line” guidance approach in Ref. 2. In this method one or more lines intersecting the Earth are established. The final dive-line intersects the target, and its direction can be set to the desired direction. The vehicle’s velocity vector is then steered toward the dive-lines by a cross-product guidance law. Another guidance method discussed in Ref. 3 fits a single-segment cubic spline between the current vehicle position and the target location, assuming

that the vehicle's motion is constrained to lie in a vertical plane. The value of the final flight path angle is one of the parameters that are used to define the cubic spline. The vehicle then is guided to follow this cubic curve. Under the assumption of perfect tracking, the final flight path angle will be as required (there is, however, no mechanism to control the azimuth of the final trajectory of the vehicle). Yet the numerical experiments reported in Ref. 4 suggest that the accuracy of these two methods would not be adequate for our current applications. Under the linearization approximation, a planar engagement problem with a final impact angle constraint is formulated as a numerical optimal control problem in Ref. 5 where the impact angle constraint is treated as a penalty term. Aside from the linearization limitations, it is not clear how realistic the computation requirements will be for such a purely numerical approach in the current applications we are considering, especially when the problem has to be solved in three-dimensional motion. Two-dimensional intercept with a final impact angle constraint is again the subject of Ref. 6. The key assumptions necessary for the analytical solution obtained therein are constant velocity and small error angles. With these conditions a time-varying bias term is added in a proportional-navigation guidance law to achieve the final impact angle condition. The constant velocity approximation is completely invalid in our current applications, since the velocity can have variations up to 60% and more.

We propose an adaptive guidance approach for the above problem in a proportional-navigation form. An earlier, non-adaptive version of the guidance law in the horizontal plane is analyzed in Ref. 7. In this paper we present the guidance law in the vertical direction, thus extending the approach to 3-dimensional (3D) flight. We provide the analysis to establish the achievement of impact on the target by the 3D guided trajectory. Unlike many other guidance approaches, we do not rely on approximations such as constant velocity or linearization. The guidance method can guide the vehicle to the target from any initial conditions in 3D space within the maneuvering capability of the vehicle. Furthermore, the properties of the guided trajectory discovered in the analysis allow us to conveniently devise guidance logic and guidance parameter selection criteria to meet the impact direction requirement. These

guidance parameters are further updated by closed-loop nonlinear adaptation laws to ensure high precision in the impact angle conditions. In this paper the word “adaptive/adaptation” is used in the context of continuously updating certain gains in a closed-loop fashion to ensure that some specified targeting conditions are accurately achieved. No estimates of unknown system parameters are involved as in a conventional adaptive control setting.

The efficacy of the proposed approach is demonstrated by the simulations of the trajectories of a hypersonic maneuvering vehicle. The terminal conditions are all met with a high degree of accuracy. Comparison with optimal solutions reveals interestingly that when the final heading angle is free, the guided trajectories and guidance commands exhibit behaviors that are quite close to those of the optimal trajectories.

II. Analysis of Guidance Laws

For development purposes, an Earth-fixed coordinate system is defined to be as shown in Fig. 1. The target is at the origin of the coordinate system. We will focus on a fixed target in the following discussion, although most of the development would be applicable to a mobile target if the motion variables in the subsequent sections are replaced by those for the relative motion between the vehicle and the target. The x -axis is pointed to the East, the y -axis to the North, and the z -axis completes the right-hand system. The line-of-sight (LOS) from the target to the vehicle is defined by the azimuth angle θ and elevation angle ϕ , where $-\pi \leq \theta \leq \pi$ is measured from positive x -axis in a counterclockwise direction, and $0 \leq \phi \leq \pi/2$. These angles can be calculated from the known coordinates of the target and navigation-derived coordinates of the vehicle.

The standard 3-dimensional equations of motion of a gliding vehicle over a flat Earth can

be found in, for instance, Ref. 8

$$\dot{x} = V \cos \gamma \sin \psi \quad (1)$$

$$\dot{y} = V \cos \gamma \cos \psi \quad (2)$$

$$\dot{z} = V \sin \gamma \quad (3)$$

$$\dot{V} = -\frac{D}{m} - g \sin \gamma \quad (4)$$

$$\dot{\gamma} = \frac{L \cos \sigma}{mV} - \frac{g}{V} \cos \gamma \quad (5)$$

$$\dot{\psi} = \frac{L \sin \sigma}{mV \cos \gamma} \quad (6)$$

where the position coordinates are x , y , and z . The Earth-relative velocity is V . The flight path angle γ is the angle between the relative velocity vector and the horizontal plane. The vehicle heading angle ψ is the angle between the horizontal projection of the velocity vector and north, measured in a clockwise direction in the horizontal plane. We choose to limit the range of ψ by $-\pi \leq \psi \leq \pi$. The gravity acceleration $g = 9.81 \text{ m/s}^2$ is treated as a constant. Since only unpowered flight is considered, the vehicle mass is also a constant. The terms D and L are the aerodynamic drag and lift forces which are dependent on the angle of attack α , altitude z and velocity V . The bank angle of the vehicle is σ .

By the definition of the coordinate system, the target is at the origin. Suppose that Ψ_f and Γ_f are the heading angle and flight path angle, respectively, that define the desired impact direction of the vehicle just before it reaches the target (cf. Fig. 1). Therefore the vehicle needs to achieve the following final conditions

$$x_f = y_f = z_f = 0 \quad (7)$$

$$\gamma_f = \Gamma_f \quad (8)$$

$$\psi_f = \Psi_f \quad (9)$$

One special case is when $\Gamma_f = -90 \text{ deg}$ (vertical impact). In such a case the constraint (9) must be removed because ψ_f is not defined for vertical impact. It should be stressed,

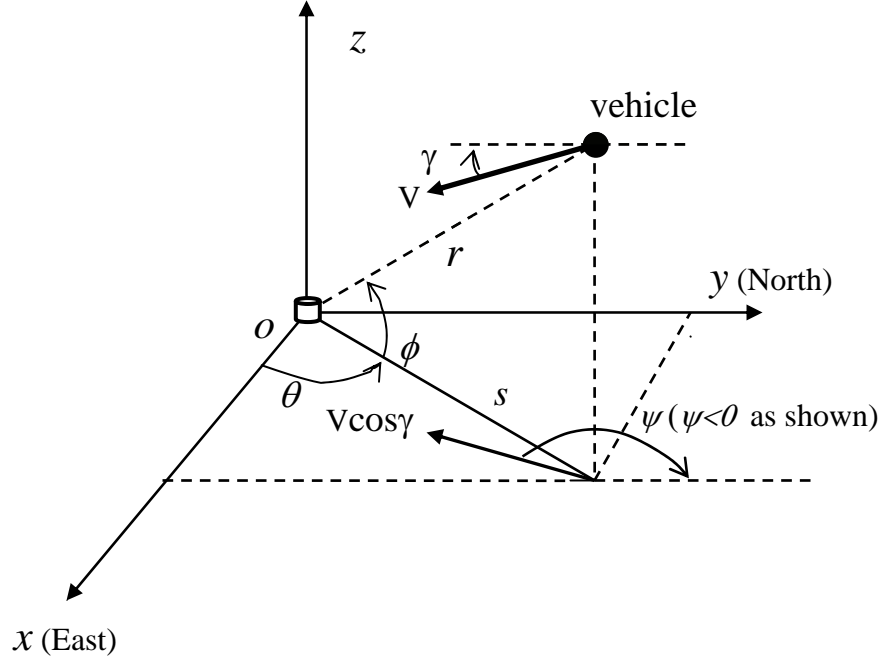


Figure 1: Coordinate system and geometry (both $\gamma < 0$ and $\psi < 0$ as shown)

however, that the vehicle's turning capability usually is the limiting factor for how much final heading adjustment, as defined in Eq. (9) can be achieved. This is because in the application scenarios under consideration the vehicle is flying at hypersonic speeds. At such speeds the vehicle cannot make significant heading changes in a short period of time. Therefore the initial conditions for the terminal guidance phase should be such that it is feasible for the vehicle to achieve the terminal conditions (7)-(9) subject to its maneuverability constraints.

The function of the terminal guidance system is to determine the direction of the flight, defined by γ and ψ , to achieve the required final conditions (7)-(9). We propose the following proportional-navigation guidance laws for the commanded heading angle ψ_{com} and flight path angle γ_{com}

$$\dot{\psi}_{com} = -\lambda_1 \dot{\theta} \quad (10)$$

$$\dot{\gamma}_{com} = -\lambda_2 \dot{\phi} \quad (11)$$

where the guidance parameters λ_1 and λ_2 are taken to be constants in this section unless

otherwise specified. The horizontal guidance law (10) is fully analyzed in Ref. 7, where it is assumed that the vehicle can track the guidance command perfectly, i.e., $\psi \equiv \psi_{com}$. The following two key properties of the guidance law (10) have been established:⁷

1. For arbitrary variations of V and $|\gamma| < 90$ deg, and for any initial conditions except for $\theta(0) + \psi(0) = \pi/2$, the guidance law (10) with $\lambda_1 > 1$ ensures that $s = \sqrt{x^2 + y^2} \rightarrow 0$. The only exception of $\theta(0) + \psi(0) = \pi/2$ corresponds to the case where the vehicle flies away from the target along the LOS from the target to the vehicle, a pathological case that will not happen in reality.
2. For all $\lambda_1 > 2$, the trajectory of the vehicle on the xy -plane will converge to a straight line passing through the origin (target) with a configuration of $\theta + \psi = -\pi/2$.

The analysis of the vertical guidance law (11) will be greatly simplified when the second property above is taken into consideration. Suppose that a $\lambda_1 > 2$ is used. After an initial transient period, the 3-dimensional trajectory of the vehicle will practically be confined in a vertical plane containing the origin, and the velocity vector projection on the xy -plane will be directed toward the origin. In this vertical plane the kinematics of the vehicle may be represented by

$$\dot{z} = V \sin \gamma \tag{12}$$

$$\dot{s} = -V \cos \gamma \tag{13}$$

where once again, $s = \sqrt{x^2 + y^2}$ is the range-to-go. The reader is referred to Fig. 1 for the geometry, with the reminder that the horizontal velocity component $V \cos \gamma$ now points to the origin. The elevation angle ϕ then is determined by

$$\phi = \tan^{-1} \left(\frac{z}{s} \right) \tag{14}$$

Using Eqs. (12) and (13), the derivative of ϕ can be readily found to be

$$\dot{\phi} = \frac{V}{r} \sin(\phi + \gamma) \tag{15}$$

where $r = \sqrt{s^2 + z^2} = \sqrt{x^2 + y^2 + z^2}$. The derivative of r is also easily obtained

$$\dot{r} = -V \cos(\phi + \gamma) \quad (16)$$

Define

$$\eta = \phi + \gamma \quad (17)$$

Then $\dot{\eta} = \dot{\phi} + \dot{\gamma}$. Again let us assume perfect tracking of the guidance command so that $\dot{\gamma} = \dot{\gamma}_{com}$. By the guidance law (11) and Eq. (15)

$$\dot{\eta} = \dot{\phi} + \dot{\gamma} = (1 - \lambda_2)\dot{\phi} = (1 - \lambda_2)\frac{V}{r} \sin \eta \quad (18)$$

Dividing Eq. (16) by Eq. (18) results in

$$\frac{dr}{d\eta} = \frac{1}{(\lambda_2 - 1)} \frac{r \cos \eta}{\sin \eta} \quad (19)$$

Upon integration, the above equation yields

$$r = c |\sin \eta|^{\frac{1}{\lambda_2 - 1}} \quad (20)$$

where $c > 0$ is an integration constant. Consider the case of $0 < \eta(0) < \pi$ for the moment.

Substituting Eq. (20) into Eq. (18) gives

$$\dot{\eta} = \frac{(1 - \lambda_2)V}{c} (\sin \eta)^{\frac{\lambda_2 - 2}{\lambda_2 - 1}} \quad (21)$$

For any chosen λ_2 , the sign of $\dot{\eta}$ will remain unchanged for all $t \geq 0$. In particular $\dot{\eta} < 0$ and η will continue to decrease to zero if $\lambda_2 > 1$. In such a case the solution of r in Eq. (20) indicates that $r \rightarrow 0$ when $\eta \rightarrow 0$. Moreover, Eq. (21) also reveals that $\dot{\eta} \rightarrow 0$ as $\eta \rightarrow 0$ if $\lambda_2 > 2$. Since $\dot{\eta} = (1 - \lambda_2)\dot{\phi}$, $\dot{\eta} \rightarrow 0 \Rightarrow \dot{\phi} \rightarrow 0$. Hence ϕ approaches a constant and γ approaches the negative of the same constant. This means that the trajectory in the vertical sz -plane converges to a straight line passing through the origin with $\gamma = -\phi$. A similar analysis leads to the same conclusions in the case where $-\pi < \eta(0) < 0$.

Combining the above analysis and the results in Ref. 7, we have the following conclusions for guidance laws (10) and (11)

1. For arbitrary variations of V , the guidance laws (10) with $\lambda_1 > 1$ and guidance law (11) with $\lambda_2 > 1$ ensure that $r = \sqrt{x^2 + y^2 + z^2} \rightarrow 0$.
2. For $\lambda_1 > 2$ and $\lambda_2 > 2$, the 3D trajectory of the vehicle will converge to a straight line passing through the origin (target) with the configuration of $\theta + \psi = -\pi/2$ and $\phi + \gamma = 0$.

Note that even though the guidance laws (10) and (11) are decoupled in two independent channels, the above analysis establishes the simultaneous satisfaction of the 3 impact conditions in Eq. (7), since $r = \sqrt{x^2 + y^2 + z^2} \rightarrow 0$ is the result. No less noteworthy is the fact that the analysis and global convergence results of the guidance laws (10) and (11) in the 3D space do not require any assumptions of small perturbations or constant velocity, as is usually required in many other approaches.

It is not difficult to show that if λ_2 is not a constant, but time-varying, Eq. (19) can still be integrated by parts to arrive at a result similar to Eq. (20). The difference is that the constant c in Eqs. (20) and (21) is replaced by a positive function ce^ξ where

$$\xi = \int \frac{\ln |\sin \eta|}{(\lambda_2 - 1)^2} d\lambda_2 \quad (22)$$

The presence of the positive variable e^ξ in Eqs. (20) and (21) does not alter the preceding analysis, therefore the results remain valid for λ_2 that is time-varying. A subtle point in this case is that the above integral is defined only for $\eta \neq 0$. This is just an artifact of using η as the independent variable in integrating Eq. (19), not an indication of an inherent problem with time-varying λ_2 . In fact, employing the standard stability theory,⁹ one can show that starting from any initial condition $|\eta_0| < \pi$, $\eta \rightarrow 0$ for any time-varying $\lambda_2 > 1$ in Eq. (18). As $\eta \rightarrow 0$, \dot{r} from Eq. (16) will remain negative, hence $r \rightarrow 0$. A parallel argument will apply to a time-varying λ_1 in the lateral guidance law (10). In conclusion the analysis and results given above are still correct even for time-varying λ_1 and λ_2 . This conclusion will be the basis for the validity of the guidance laws when λ_1 and λ_2 are continuously updated by adaptation laws, as will be discussed in Section IV.

III. Terminal Guidance Logic

A. Guidance Parameter Selections

While other types of interceptor guidance approaches exist that can target the typical final conditions in Eq. (7), few can conveniently handle the unique final conditions Eqs. (8) and (9). Guidance laws (10) and (11), on the other hand, offer simple ways to address these requirements by properly selecting the guidance parameters λ_1 and λ_2 . To see this, we integrate the guidance equation $\dot{\psi}_{com} = -\lambda_1\dot{\theta}$ from t_0 to t with the assumption of perfect tracking $\dot{\psi} = \dot{\psi}_{com}$

$$\psi - \psi_0 = -\lambda_1(\theta - \theta_0) \quad (23)$$

where ψ_0 and θ_0 are the conditions at t_0 which is the first instant when the guidance law (10) is applied. Suppose that $\lambda_1 > 2$. By the above discussion the steady-state configuration is

$$\theta_{ss} + \psi_{ss} = -\pi/2 \quad (24)$$

Let $\psi_{ss} = \Psi_f$ as desired. Then the corresponding steady-state value for θ is

$$\Theta_f = -\pi/2 - \Psi_f \quad (25)$$

Replacing ψ by Ψ_f and θ by Θ_f in Eq. (23), we can solve for the unique value of λ_1 required to achieve $\psi_{ss} = \Psi_f$

$$\lambda_1 = -\frac{\Psi_f - \psi_0}{\Theta_f - \theta_0} = 1 + \frac{\delta\psi_0}{\Theta_f - \theta_0} \quad (26)$$

where

$$\delta\psi_0 = \psi_0 - \left(-\frac{\pi}{2} - \theta_0\right) \quad (27)$$

The quantity $\delta\psi_0$ defined above is simply the initial heading offset of the vehicle with respect to the origin (target). To recap the discussion, if the value of λ_1 given by Eq. (26) is greater than 2, this λ_1 will ensure that the final condition (9) is met. Of course the right hand side of Eq. (26) may be less than 2 at t_0 . When this happens, a simple strategy will be discussed

later to fly the vehicle until the right hand side of Eq. (26) is greater than 2 with the current value of θ and $\delta\psi$ in place of θ_0 and $\delta\psi_0$. From this point on the guidance law (10) with the λ_1 value calculated from Eq. (26) is applied.

A similar discussion applies to guidance law (11). Integrating the guidance equation $\dot{\gamma}_{com} = -\lambda_2\dot{\phi}$ with the assumption of perfect tracking $\dot{\gamma} = \dot{\gamma}_{com}$ gives

$$\gamma - \gamma_0 = -\lambda_2(\phi - \phi_0) \quad (28)$$

where γ_0 and ϕ_0 are the initial conditions at t_0 (where it is understood that this t_0 is not necessarily the same t_0 as in the above case). Suppose that $\lambda_2 > 2$. By the analysis in the preceding section the trajectory will converge to the configuration where $\gamma = -\phi \rightarrow \gamma_{ss}$ for some steady-state value of γ_{ss} . If we require that $\gamma_{ss} = \Gamma_f$, Eq. (28) dictates that the corresponding λ_2 must satisfy

$$\lambda_2 = \frac{\Gamma_f - \gamma_0}{\Gamma_f + \phi_0} \quad (29)$$

provided that $\lambda_2 > 2$ is also met by the result. For steep impact (Γ_f close to or equal to -90 deg), the right hand side of Eq. (29) will become greater than 2 only after the vehicle gets close to the target. Thus a strategy is again to continuously evaluate the value of the right hand side of Eq. (29) with the current values of γ and ϕ in place of γ_0 and ϕ_0 . Once the computed value is greater than 2, the guidance law (11) is activated with this value for λ_2 for the rest of the flight. The λ_2 so computed on-board will ensure the satisfaction of the terminal condition (8) in the guidance.

B. Lateral Guidance Logic

The analysis in Section II suggests the sequence in which the terminal guidance logic should work: the lateral guidance will first align the heading of the vehicle nearly toward the target; then the longitudinal guidance will work to bring the flight path angle to the required value while steering the vehicle to the target, while the lateral guidance maintains the correct heading. The following lateral guidance logic is designed for the heading alignment.

1. If $\Gamma_f = -90$ deg in the constraint (8) or constraint (9) is *not* imposed, a constant $\lambda_1 > 2$ is used throughout the entire trajectory in the guidance law (10) which is responsible for the lateral steering.
2. If $\Gamma_f \neq -90$ deg, constraint (9) is imposed, and the λ_1 calculated from Eq. (26) at the guidance initiation is less than 2, the bank angle of the vehicle is commanded by

$$\sigma_{com} = \sigma_{max} \text{sgn}(\Theta_f - \theta) \quad (30)$$

where Θ_f is given in Eq. (25) and θ is the current value of the variable. The sign function $\text{sgn}(x) = 1$ when $x > 0$, and $\text{sgn}(x) = -1$ when $x < 0$. The pre-set limit $\sigma_{max} \in (0, 90)$ deg is a maximum bank angle to be used for turning. While the command (30) is applied, the value of λ_1 computed from Eq. (26) is continuously monitored with $\delta\psi_0$ and θ_0 replaced by their current values. At the moment when the λ_1 so computed is greater than 2, the current time is set to be t_0 , and the guidance logic is switched to Step 3 below for the rest of the trajectory.

3. If $\Gamma_f \neq -90$ deg, constraint (9) is imposed, and the λ_1 calculated from Eq. (26) at t_0 is greater than 2, this λ_1 is used in the guidance law (10) for the rest of the terminal phase flight.

A discussion on the above lateral guidance logic is in order. Step 1 is the simple case where the constraint (9) is not required. Thus a $\lambda_1 > 2$ in the guidance law (10) will suffice according to the conclusions in Section II. When the constraint (9) is enforced, the lateral guidance logic should always end in Step 3, for the selection of λ_1 described in Step 3 ensures the satisfaction of condition (9). The analysis below establishes that even if the trajectory starts in Step 2, the logic will eventually switch into Step 3.

From the definition of $\theta = \tan^{-1}(y/x)$ and Eqs. (1-2), it is easy to show that

$$\frac{d(\Theta_f - \theta)}{dt} = -\dot{\theta} = -\frac{V \cos \gamma \sin \delta\psi}{s} \quad (31)$$

where $\delta\psi = \psi - (-\pi/2 - \theta)$. From Eq. (6) and the above equation, we also have

$$\delta\dot{\psi} = \frac{L \sin \sigma}{mV \cos \psi} + \frac{V \cos \gamma \sin \delta\psi}{s} \quad (32)$$

Equation (31) indicates that the rate of $\Theta_f - \theta$ is essentially proportional to $\delta\psi$ for small $|\delta\psi|$. Hence $\Theta_f - \theta$ is a slower variable and $\delta\psi$ is a faster variable with respect to any changes in σ . It can be shown that the bank angle command law in Eq. (30) will always increase the ratio

$$\frac{\delta\psi}{\Theta_f - \theta}$$

in all practically possible cases. Therefore as this ratio increases, there will be an instant when it is greater than 1, and the λ_1 computed from Eq. (26) becomes greater than 2, where $\delta\psi_0 = \delta\psi$ and $\theta_0 = \theta$ are used in Eq. (26). Thus Step 2 in the above logic will eventually lead to Step 3. This conclusion, of course, is contingent on the condition that there is sufficient time for the vehicle to make the turn. Alternatively, the misalignment in the velocity heading should not be too large to overcome in a reasonable time period compared with the flight time in the terminal phase.

It should be commented that the bank angle given by Eq. (30) for the initial turning is neither unique nor necessarily optimal for a given case. Depending on the initial conditions, there may be different bank angle profiles in this initial turn, possibly even with opposite sign than the sign determined in Eq. (30), that can still allow the vehicle to meet its final heading requirement (see an example in Section IV). But the determination of such alternate bank angle will require repeated numerical integrations of the equations of motion for the vehicle. What the strategy in (30) offers is simplicity and assured eventual achievement of $\lambda_1 > 2$ as computed from Eq. (26), a key requirement in our guidance approach.

The above lateral guidance logic is included in the flow chart in Fig. 2. The other parts of the chart, the computation of bank angle/angle of attack commands and further adaptation of λ_1 , will be discussed in Sections III-D and IV.

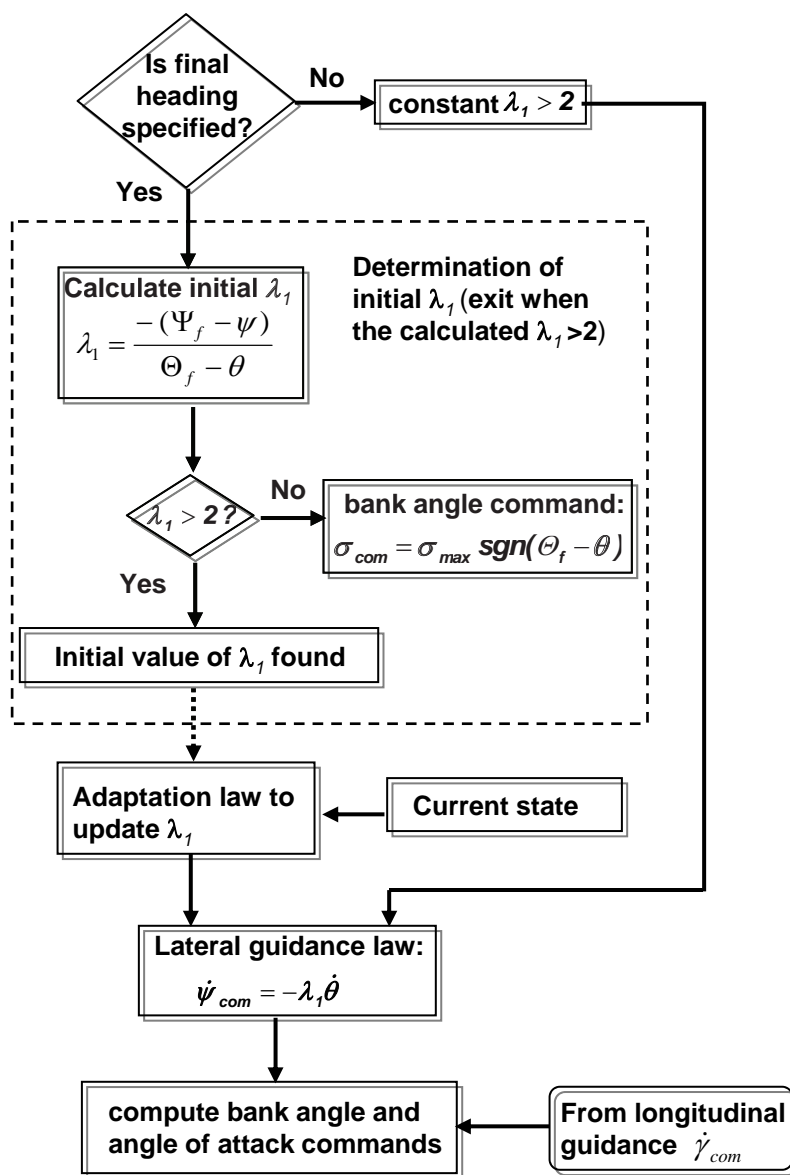


Figure 2: Flow chart for the lateral guidance logic

C. Longitudinal Guidance Logic

Once the lateral guidance logic has nearly aligned the heading of the vehicle to the target, the longitudinal guidance logic will begin to work toward achieving the impact conditions (7) and (8). As in the case of lateral guidance, certain logic in addition to guidance law (11) will be needed, which is mainly driven by the condition (8) and the desire to maximize the impact velocity. Recall that the analysis in Ref. 7 has shown that under guidance law (10) the angle ψ will approach $-\pi/2 - \theta$ monotonically. For the purpose of longitudinal guidance activation, the end of the heading alignment phase under Step 1 or Step 3 in the lateral guidance logic may be marked by the condition

$$|\delta\psi| = \left| \psi + \Theta_f + \frac{\pi}{2} \right| \leq \varepsilon \quad (33)$$

where $\varepsilon > 0$ is a small pre-specified constant. When the constraint (9) is not imposed, the above condition is replaced by

$$|\delta\psi| = \left| \psi + \theta + \frac{\pi}{2} \right| \leq \varepsilon \quad (34)$$

The following sequential longitudinal guidance logic is devised:

1. From the beginning of the terminal guidance phase at $t = 0$ to the end of the heading alignment phase, the vehicle will fly an angle of attack profile defined by

$$\alpha_{trans} = \alpha^* + (\alpha_0 - \alpha^*)e^{-t/T} \quad (35)$$

where α_0 is the angle of attack of the vehicle at $t = 0$, and α^* is the angle of attack at which the vehicle achieves its maximum lift-to-drag (L/D) ratio (α^* can be a function of Mach number if needed). The time constant $T > 0$ is a pre-selected parameter to ensure reasonably fast transition from α_0 to α^* .

2. From the end of the heading alignment phase to the point where the right hand side of Eq. (29) becomes greater than 2, a $\lambda_2 < 1$ is used in guidance law (11).

3. After the instant when the λ_2 calculated from Eq. (29) is greater than 2, this value of λ_2 is used in guidance law (11) until the impact (λ_2 remains the same value in this period)

While the vehicle is turning in the heading alignment phase, the objective for flying the transition angle of attack profile in Eq. (35) is to preserve the energy of the vehicle so that the impact velocity can be close to the maximum possible value. This maneuver turns out to be quite similar to what an optimal trajectory would do, as will be seen later. In the second step of the above logic, the vehicle prepares for the final maneuver to the target. It is in this phase where the guidance law (11) begins to drive the α to decrease from close to α^* to a negative value (we assume that the magnitude of the bank angle is limited within 90 deg). The value of λ_2 should be moderate in this period, for an overly aggressive flight path angle command could result in a very late occurrence of $\lambda_2 > 2$ from Eq. (29), leaving little time for the final maneuver to satisfy the condition (8). Note that a $\lambda_2 < 1$ can be used in this phase even though the analysis in Section II states that $\lambda_2 > 1$ is needed for $r \rightarrow 0$. This is because $\eta = \phi + \gamma$ is typically positive and less than $\pi/2$ ($|\gamma|$ is still rather small) in this period. By examining Eqs. (20) and (21), we can show that even for $\lambda_2 < 1$, η will increase and r will decrease, only not to zero. But we only need r to decrease in this phase. The last phase fulfills the requirement for the satisfaction of the impact condition (8). Note that the lateral guidance law (10) with a constant $\lambda_1 > 2$ remains in force throughout all the above longitudinal logic steps.

The above longitudinal guidance logic is incorporated in the flow chart in Fig. 3. The other components of Fig. 3, including the computation of bank angle/angle of attack commands and adaptation of λ_1 and λ_2 , will be discussed in the next section and Section IV.

D. Bank Angle and Angle of Attack Commands

The realization of the guidance commands from Eqs. (10) and (11) can be through the modulations of bank angle σ and angle of attack α which in turn will affect the vehicle

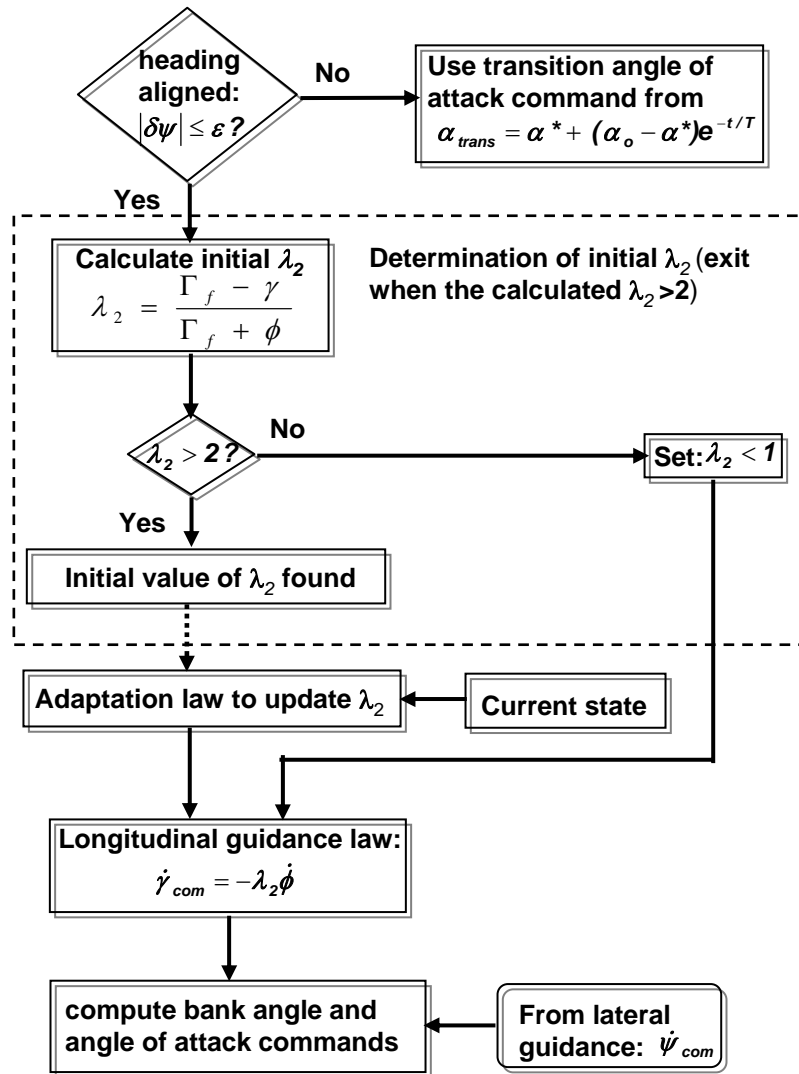


Figure 3: Flow chart for the longitudinal guidance logic

dynamics Eqs. (4-6). To compute the required bank angle command σ_{com} and α -command α_{com} , we first find the required aerodynamic lift force to generate the guidance commands $\dot{\psi}_{com}$ and $\dot{\gamma}_{com}$ from Eqs. (5) and (6)

$$\frac{L_{com}}{m} = \text{sgn}(V\dot{\gamma}_{com} + g \cos \gamma) \sqrt{(V\dot{\psi}_{com} \cos \gamma)^2 + (V\dot{\gamma}_{com} + g \cos \gamma)^2} \quad (36)$$

The sign function in the above equation determines whether a positive or negative lift force is commanded (again, with the assumption of $|\sigma| < 90$ deg). Let $C_{L_{com}}$ be the lift coefficient required to produce L_{com} . Therefore

$$\frac{1}{2}\rho(z)V^2S_{ref}C_{L_{com}} = L_{com} \quad (37)$$

where ρ is the atmospheric density as a function of altitude z , and S_{ref} the reference area of the vehicle. Based on the required $C_{L_{com}}$ found in the above equation, the aerodynamic model of the vehicle is iterated to solve for the corresponding angle of attack α_{com} at the current Mach number.

The commanded bank angle σ_{com} is calculated from Eq. (6) with $\dot{\psi}$ replaced by $\dot{\psi}_{com}$ and L replaced by L_{com}

$$\sigma_{com} = \sin^{-1} \left(\frac{mV\dot{\psi}_{com} \cos \gamma}{L_{com}} \right) \quad (38)$$

In the case where the value of $C_{L_{com}}$ computed from Eq. (37) demands an α_{com} that is beyond the allowable range for the vehicle, a scaling of the guidance commands may be done. Suppose that \bar{L}_{max} represents the largest lift force feasible at the current condition (which can be in the positive or negative direction, depending on the sign of $(V\dot{\gamma}_{com} + g \cos \gamma)$). Let both $\dot{\psi}_{com}$ and $\dot{\gamma}_{com}$ be scaled by $K_{max} > 0$ so that the total resulting lift force is equal to \bar{L}_{max} . To determine K_{max} , replace $\dot{\psi}_{com}$ and $\dot{\gamma}_{com}$ by $K_{max}\dot{\psi}_{com}$ and $K_{max}\dot{\gamma}_{com}$, and L_{com} by \bar{L}_{max} in Eq. (36). The value of K_{max} is the positive root of the quadratic equation

$$K_{max}^2 \left[V^2(\dot{\psi}_{com}^2 \cos^2 \gamma + \dot{\gamma}_{com}^2) \right] + K_{max}(2Vg\dot{\gamma}_{com} \cos \gamma) + \left[g^2 \cos^2 \gamma - \frac{\bar{L}_{max}^2}{m^2} \right] = 0 \quad (39)$$

A solution of $K_{max} < 1$ indicates that the guidance commands exceed the vehicle's capability. The guidance commands in both channels in such a case need to be scaled back by the same

factor of K_{max} . Alternatively, separate scaling of each channel could be performed. Let $K_\psi > 0$ and $K_\gamma > 0$ be the weightings on $\dot{\psi}_{com}$ and $\dot{\gamma}_{com}$, respectively. Within the current limit of the lift, the emphasis of the guidance can be directed in one channel at the expense of less guidance effort in the other channel. For instance, we may express K_ψ by using Eq. (36) with the substitutions of $\dot{\psi}_{com}$ and $\dot{\gamma}_{com}$ by $K_\psi\dot{\psi}_{com}$ and $K_\gamma\dot{\gamma}_{com}$, and L_{com} by \bar{L}_{max}

$$K_\psi = \frac{1}{|\dot{\psi}_{com}|V \cos \gamma} \sqrt{\frac{\bar{L}_{max}^2}{m^2} - (K_\gamma V \dot{\gamma}_{com} + g \cos \gamma)^2} \quad (40)$$

The selection of a $K_\gamma \leq K_{max}$ will result in a $K_\psi \geq K_{max}$, placing more emphasis on the heading control than on flight path angle control. The reverse is also true.

In the event when $|L_{com}| > |\bar{L}_{max}|$, and once the scaling factors have been determined, the angle of attack and bank angle commands are still computed from Eqs. (37) and (38), only with L_{com} replaced by \bar{L}_{max} and $\dot{\psi}_{com}$ by $K_\psi\dot{\psi}_{com}$.

E. Body Acceleration Commands

Another option for flight control system to realize the guidance commands generated by the guidance laws (10) and (11) is to track appropriate body acceleration commands. The advantage of this design is that the feedback of the controlled variables (accelerations) can be directly provided by accelerometers. The guidance system will determine the acceleration commands to be tracked so that the velocity vector is steered according to Eqs. (10) and (11).

Define a velocity frame which has its unit vectors as

$$\mathbf{i}_v = \frac{\mathbf{V}}{V} \quad (41)$$

$$\mathbf{j}_v = \frac{\mathbf{V} \times \mathbf{R}}{\|\mathbf{V} \times \mathbf{R}\|} \quad (42)$$

$$\mathbf{k}_v = \mathbf{i}_v \times \mathbf{j}_v \quad (43)$$

where \mathbf{V} is the relative velocity vector and \mathbf{R} is the radius vector from the center of the

Earth to the vehicle. The vehicle's acceleration in this velocity frame is given by

$$\mathbf{a} = \dot{V}\mathbf{i}_v + \dot{\psi}V \cos \gamma \mathbf{j}_v - \dot{\gamma}V\mathbf{k}_v \quad (44)$$

The body frame fixed to the vehicle is defined in standard convention: the x_b -axis coincides with the body longitudinal axis, the z_b -axis points down, and the y_b -axis completes the right hand system. With the assumption of zero sideslip, the coordinate transformation from the velocity frame to the body frame consists of a sequence of two rotations. The first is the rotation of a bank angle σ about the velocity vector (\mathbf{i}_v direction); the second an angle of attack α about the y_b -axis. Using the coordinate transformation and the expression of the acceleration in the velocity frame in Eq. (44), we obtain the corresponding commanded body accelerations (including gravity) in the y_b and z_b axes as

$$n_{y_{com}} = \dot{\psi}_{com}V \cos \gamma \cos \sigma_{com} - \dot{\gamma}_{com}V \sin \sigma_{com} \quad (45)$$

$$n_{z_{com}} = \dot{V}_{com} \sin \alpha_{com} - \dot{\psi}_{com}V \cos \gamma \cos \alpha_{com} \sin \sigma_{com} - \dot{\gamma}_{com}V \cos \alpha_{com} \cos \sigma_{com} \quad (46)$$

where $\dot{\psi}_{com}$ and $\dot{\gamma}_{com}$ are from the guidance laws (10) and (11), and σ_{com} and α_{com} are computed in Section III-D above. The value of \dot{V}_{com} is from the right hand side of Eq. (4) with $\alpha = \alpha_{com}$ in calculating the drag force term D . The command inputs to the control system in the inner loop will thus be $n_{y_{com}}$ and $n_{z_{com}}$. Note that only when $\alpha_{com} \approx 0$ and $\sigma_{com} \approx 0$ can $n_{y_{com}}$ and $n_{z_{com}}$ be approximated by

$$n_{y_{com}} = \dot{\psi}_{com}V \cos \gamma \quad (47)$$

$$n_{z_{com}} = -\dot{\gamma}_{com}V \quad (48)$$

IV. Adaptive Update of Guidance Parameters

Assuming perfect navigation data, the above proposed guidance approach typically renders a precision of within 1 meter on impact position. The impact angle conditions can be met in many cases within 1 deg. But in some other cases the errors could reach as high as 3

to 4 degrees. The possible sources of errors include: (1) the guidance commands briefly exceed the maneuverability of the vehicle; (2) the rate and acceleration limits on the guidance commands are momentarily saturated; (3) the analyses are based on steady-state conditions, yet the the flight is relatively short so the steady state has not been fully achieved at the termination of flight; (4) appreciable aerodynamic uncertainty exists, due to either modeling mismatch or the effects of ablation sustained during entry flight; (5) the analyses of the guidance laws are based only on point-mass dynamics, and the guidance parameter selections assume perfect tracking of the guidance commands; (6) the guidance commands are only updated at a finite rate. Adding to the sources of errors in an operational environment will be limited navigation resolution, winds, and modeling uncertainties. Most of these issues are present to one degree or another in all other guidance and control law synthesis efforts, and most of the time their influences on the performance of the system are secondary. But in the case of very high-precision applications such as discussed in this paper, their effects become non-trivial.

In the guidance logic developed so far, the two parameters λ_1 and λ_2 are constants once their values are determined (even though by on-line calculations from Eqs. (26) and (29)). Recall that these values are selected on the basis of satisfying the impact angle conditions. But any of the above possible reasons can cause the actual trajectory to be different, thus the already determined constant values of λ_1 and λ_2 may no longer ensure the precision of the impact angle conditions. The application scenarios considered in this paper rule out the options of adopting more elaborate guidance means or relying on intensive on-line computation for guidance command generation. Within the framework of the current approach, an effective way to further enhance the precision is appropriate closed-loop adaptation for λ_1 and λ_2 . We present in the following a novel approach to establish the adaptive update laws for the problem at hand.

Let us consider the vertical guidance law (11) first. We will use the altitude z as the independent variable for the update of λ_2 . Note that Eq. (11) has the same form whether

the differentiation is with respect to time or altitude (or any other independent variable). Treat λ_2 as a z -dependent function instead of a constant. Integrating both sides of Eq. (11) once, the right hand side by parts, one obtains

$$\gamma - \gamma_0 = -\lambda_2\phi + \lambda_{20}\phi_0 + \int_{z_0}^z \phi\lambda_2' dz \quad (49)$$

where z_0 is an arbitrary initial altitude, z a later altitude, and $\lambda_2' = d\lambda_2/dz$. The subscript “0” indicates the values at z_0 . Suppose that λ_2 remains greater than 2 even though it is varying. From the conclusion at the end of Section II we know that as $z \rightarrow 0$, $\gamma + \phi \rightarrow 0$. With a given initial value for λ_2 , we want to find λ_2' so that $\gamma \rightarrow \Gamma_f$, thus $\phi \rightarrow -\Gamma_f$. In addition, we will seek the simplest form of update of λ_2 so λ_2' is a constant. As a result, at $z = 0$ we have $\lambda_2 = \lambda_{20} - z_0\lambda_2'$. At $z = 0$, the substitution of these conditions into Eq. (49) produces

$$\Gamma_f - \gamma_0 = (\lambda_{20} - z_0\lambda_2')\Gamma_f + \lambda_{20}\phi_0 + \lambda_2' \int_{z_0}^0 \phi dz \quad (50)$$

Since $\phi = \phi_0$ at z_0 and $\phi = -\Gamma_f$ at $z = 0$, the integral in above equation is further approximated by the well-known trapezoidal rule for quadratures

$$\int_{z_0}^0 \phi dz \approx \frac{1}{2}(\Gamma_f - \phi_0)z_0 \quad (51)$$

Replace the integral in Eq. (50) by the above relationship, and solve for λ_2'

$$\lambda_2' = -2 \frac{[(1 - \lambda_{20})\Gamma_f - \gamma_0 - \lambda_{20}\phi_0]}{z_0(\phi_0 + \Gamma_f)} \quad (52)$$

Since z_0 is arbitrary, we can let z_0 be the current altitude at any instant and drop all the subscripts 0 in the above equation. Moreover, the coefficient 2 in the above equation may be replaced by a constant gain $\kappa_2 > 0$ to allow the flexibility of tuning for desired adaptation rate. Recall that the differentiation in the above equation is with respect to the altitude z . Our final closed-loop adaptation law for λ_2 is

$$\frac{d\lambda_2}{dz} = -\kappa_2 \frac{[(1 - \lambda_2)\Gamma_f - \gamma - \lambda_2\phi]}{z(\phi + \Gamma_f)} = \frac{\kappa_2}{z} \left(\lambda_2 + \frac{\Delta\gamma}{\Delta\phi} \right) \quad (53)$$

where

$$\Delta\phi = (-\Gamma_f) - \phi, \quad \Delta\gamma = \Gamma_f - \gamma \quad (54)$$

If for any reason the adaptation with time as the independent variable is preferred, the adaptation law is simply

$$\dot{\lambda}_2 = \frac{\kappa_2}{z} V \sin \gamma \left(\lambda_2 + \frac{\Delta\gamma}{\Delta\phi} \right) \quad (55)$$

It is worth noting that one would not be able to derive adaptation law (55) if time is used as the independent variable at the outset.

In Step 3 of the longitudinal guidance logic, the starting value for λ_2 is determined by Eq. (29) at the instant when the right hand side of Eq. (29) becomes greater than 2. The subsequent values of λ_2 are then updated according to Eq. (53) or (55) instead of remaining at the same constant. As the trajectory approaches the desired configuration where $\Delta\phi = \Delta\gamma = 0$, it can be shown by using L'Hospital's rule and the guidance law (11) that

$$\lim_{\Delta\gamma \rightarrow 0, \Delta\phi \rightarrow 0} \left(\frac{\Delta\gamma}{\Delta\phi} \right) \rightarrow \left(\frac{\dot{\gamma}}{\dot{\phi}} \right) = -\lambda_2 \quad (56)$$

Therefore $\dot{\lambda}_2 \rightarrow 0$ by the adaptation law (55), i.e., the gain adaptation stops. The validity of the guidance law (11) under a varying λ_2 has been established at the end of Section II.

A similar process applied to the lateral guidance law (10) will lead to the update law for λ_1 as

$$\frac{d\lambda_1}{ds} = -\kappa_1 \frac{[(1 - \lambda_1)\Psi_f - \psi - \lambda_1(\theta + \pi/2)]}{s[\theta + \Psi_f + \pi/2]} = \frac{\kappa_1}{s} \left(\lambda_1 + \frac{\Delta\psi}{\Delta\theta} \right) \quad (57)$$

where

$$\Delta\theta = -(\Psi_f + \pi/2) - \theta, \quad \Delta\psi = \Psi_f - \psi \quad (58)$$

The parameter $\kappa_1 > 0$ is a constant gain, and the derivative in the adaptation law Eq. (57) is with respect to the range-to-go s . If time is desired to be the independent variable, the adaptation law is then

$$\dot{\lambda}_1 = -\frac{\kappa_1}{s} V \cos \gamma \left(\lambda_1 + \frac{\Delta\psi}{\Delta\theta} \right) \quad (59)$$

Again, it can be shown by using L'Hospital rule and guidance law (10) that as the trajectory approaches the final configuration where $\Delta\theta = \Delta\psi = 0$, we will have

$$\lim_{\Delta\theta \rightarrow 0, \Delta\psi \rightarrow 0} \left(\frac{\Delta\psi}{\Delta\theta} \right) \rightarrow \left(\frac{\dot{\psi}}{\dot{\theta}} \right) = -\lambda_1 \quad (60)$$

Thus $\dot{\lambda}_1 \rightarrow 0$ by Eq. (59), and the adaptation of λ_1 stops. The adaptation of λ_1 is not needed when the final heading constraint (9) is not imposed, because a constant $\lambda_1 > 2$ is all that is required in this case. This “bypass” is clearly shown in Fig. 2. The complete lateral and longitudinal guidance logics including the guidance parameter adaptation are illustrated in Figs. 2 and 3.

To avoid the singularities of the adaptation laws (53) and (57) at the origin where $z = s = 0$, the parameter adaptation is stopped at a distance before the origin is reached without practical impact on the precision, for the effects of the guidance parameter adaptation are diminished as the vehicle gets very close to the target.

V. Simulations

The adaptive terminal guidance logic presented in Sections II–IV is applied in simulations to the guidance of a hypersonic lifting vehicle of about 680 kg (1,500 lb) in weight. The vehicle features a bi-conic configuration with 4 control surfaces. The nonlinear aerodynamic model of the vehicle is Mach- and angle of attack-dependent. The first scenario is for vertical impact on the target, so the final heading constraint (9) is not imposed. The second example involves non-vertical impact and constrained final heading condition (9). The initial conditions for the terminal phase flight in both cases are those at the end of the simulated entry trajectories of the vehicle. The continuities in both bank angle and angle of attack from their respective values at the end of entry flight are preserved in the terminal phase trajectories. The atmospheric properties used in the simulations are based on the 1976 U.S. Standard Atmosphere.¹⁰ The 3DOF equations of motion over a rotating spherical Earth are used to simulate the vehicle trajectories. The guidance commands are generated at 2 HZ

rate and then subject to maximum allowable magnitude, rate and acceleration limits before they are applied in the simulations. Even though the assumption of perfect tracking of the guidance commands is made in the guidance law analysis, the control limits and finite guidance update rate do cause imperfect tracking in the simulations. Still the feedback nature of the guidance laws and the guidance parameter adaptation ensure excellent results as will be seen.

In both cases the corresponding open-loop optimal trajectories are also found for comparison purposes. The performance index of optimization is the maximization of the final velocity. The optimal control problem is converted to a nonlinear programming problem by parameterizing the time histories of bank angle and angle of attack with piecewise linear functions of time. The equations of motion are numerically integrated from the given initial conditions to obtain the state histories, and the final state in particular. The impact condition constraints (7), (8) and (9) (when it is imposed) are enforced. A sequential quadratic programming algorithm in MATLAB is then used to solve the nonlinear programming problem. The starting guesses to the optimization problems are completely independent of the simulated trajectories under the guidance laws.

A. Vertical Impact

In this case $\Gamma_f = -90$ deg in constraint (8), and constraint (9) is ignored. The initial conditions are given as

$$\begin{aligned}
 s_0 &= 179.387 \text{ km}, & z_0 &= 40.002 \text{ km}, & \theta_0 &= -173.14 \text{ deg} \\
 V_0 &= 2304 \text{ m/s}, & \gamma_0 &= -1.46 \text{ deg}, & \delta\psi_0 &= 5.19 \text{ deg} \\
 \sigma_0 &= 34.58 \text{ deg}, & \alpha_0 &= 28.94 \text{ deg}
 \end{aligned} \tag{61}$$

In this case a constant $\lambda_1 = 3$ is used in the lateral guidance law (10) throughout the terminal phase (Step 1 of the lateral guidance logic). It is easy to verify that the given initial conditions do not make $\lambda_2 > 2$ when λ_2 is calculated from Eq. (29). Hence the longitudinal

guidance logic steps described in Section III-C are employed to steer the trajectory in the vertical direction. For the vehicle model used, the maximum L/D ratio takes places at about $\alpha^* = 11$ deg in the range of Mach number variations during the terminal guided flight. Thus $\alpha^* = 11$ deg, and $T = 25$ s are used in Eq. (35). A value of $\lambda_2 = 0.8$ is used in Step 2 of the longitudinal guidance logic until the right hand side of Eq. (29) becomes greater than 2. The simulation stops when the altitude reduces to zero.

The final impact conditions from the simulation are

$$s_f = 0.05 \text{ m}, \quad \gamma_f = -89.97 \text{ deg}, \quad V_f = 750.7 \text{ m/s (Mach 2.21)} \quad (62)$$

It should be kept in mind that even though the above precision level in miss distance and impact angle may seem unrealistic because no navigation errors are included, the simulations are only intended to demonstrate the capability of the guidance algorithm alone. In comparison to the above final velocity in the closed-loop simulation, the open-loop optimal solution yields a final velocity of 811.1 m/s (Mach 2.38). It should be mentioned that in the optimal solutions the bank angle and angle of attack profiles are not constrained by rate and acceleration limits, which contributes (unrealistically) to the higher final velocity. Figure 4 shows the comparison of the variations of flight path angle versus altitude and Mach number versus range-to-go along the guided and optimal trajectories. The three-dimensional flight paths for both the optimal and guided trajectories are depicted in Fig. 5. Figure 6 contains the variations of bank angle and angle of attack. It is observed that, despite two completely different approaches, the qualitative behaviors of the bank angle profiles along the optimal and guided trajectories, as well as the angle of attack profiles, are remarkably similar. At about 45 seconds into the terminal phase flight, the right hand side of Eq. (29) becomes greater than 2, and λ_2 is switched from 0.8 to this value. The bank angle and angle of attack histories in Fig. 6 clearly indicate this change. Remarkably, the optimal bank angle and optimal angle of attack profiles in Fig. 6 exhibit similar transitions (a moment later) even though nothing in the formulation of the optimal control problem forces such behaviors.

The initial guesses to the optimal profiles used in the numerical optimization are not at all related to the guided trajectories.

It is shown in Ref. 11 that in one-dimensional cases, a proportional-navigation guidance law with a proportional constant of 3 approximates an optimal guidance law. The observations made here lead to an interesting conjecture: when the final heading angle is not constrained, the guidance logic developed in Section III for 3-D flight may also be made to approximate the optimal guidance solution by selecting appropriate values for the parameters in the logic (e.g., λ_1 , λ_2 , ε and T).

The guidance parameter adaptation law (53) developed in Section IV is also implemented in the simulations (λ_1 remains a constant of 3 in this case because no final heading constraint is present). A gain of $\kappa_2 = 4$ is used. At about 87 seconds into the terminal phase, the right hand side of Eq. (29) yields a value greater than 2. This is when Step 3 of the longitudinal guidance logic is activated, and the adaptation for λ_2 by Eq. (53) begins at the same time. Figure 7 shows the history of λ_2 . The changes in λ_2 are relatively small. The adaptation stops about one second before impact. The high precision of the final flight path angle shown in the final conditions (62) is representative of the effectiveness of the gain adaptation.

B. Non-Vertical Impact

The terminal values in constraints (8) and (9) are specified to be

$$\Gamma_f = -60 \text{ deg} \quad (63)$$

$$\Psi_f = 88 \text{ deg} \quad (64)$$

The initial conditions are

$$\begin{aligned} s_0 &= 366.065 \text{ km}, & z_0 &= 45.060 \text{ km}, & \theta_0 &= -172.68 \text{ deg} \\ V_0 &= 2962.67 \text{ m/s}, & \gamma_0 &= -0.87 \text{ deg}, & \delta\psi_0 &= -3.97 \text{ deg} \\ \sigma_0 &= 27.61 \text{ deg}, & \alpha_0 &= 31.74 \text{ deg} \end{aligned} \quad (65)$$

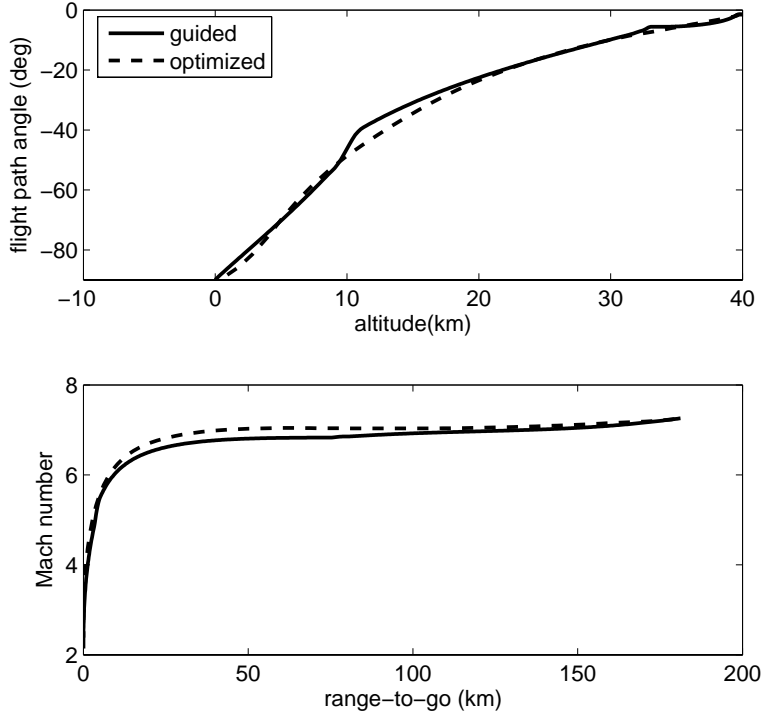


Figure 4: Flight path angle and Mach number for the vertical impact case

These initial conditions are from the same entry trajectory as in previous case, but the entry flight is terminated earlier to allow more time for the terminal phase guidance to meet the heading constraint at the impact. The above initial conditions cause the lateral guidance logic to start in Step 2 of Section III-B, and the longitudinal guidance logic in Step 2 of Section III-C. Other simulation settings and parameters are the same as in the previous case.

The final conditions of the guided trajectory in this case are

$$s_f = 0.03 \text{ m}, \quad \gamma_f = -60.02 \text{ deg}, \quad \psi_f = 88.01 \text{ deg}, \quad V_f = 943.1 \text{ m/s (Mach 2.77)} \quad (66)$$

Figure 8 shows the 3D trajectories. The ground tracks in Fig. 8 indicate that the trajectories now approach the same target from a direction different than in Fig. 5, a result of the final heading angle constraint now enforced. The optimal solution in this case gives a final velocity of 1110.7 m/s (Mach 3.26). Figure 9 reveals the reason why the guided trajectory

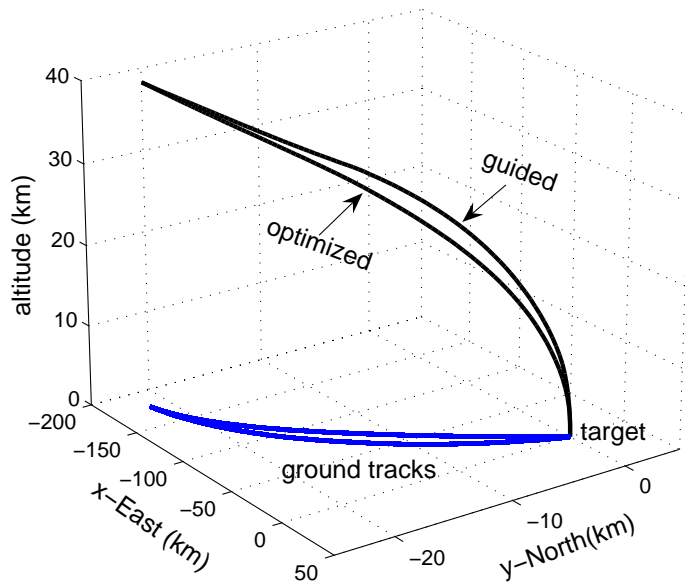


Figure 5: Three-dimensional trajectories for the vertical impact case

in this case has appreciable performance difference as compared to the optimal trajectory. Step 2 in the lateral guidance logic in this case commands initially a large negative bank angle. The optimal bank angle profile, on the other hand, decides to stay nearly constant at about +25 deg for almost 90 seconds. This is a feature that can only be discovered with extensive numerical searches required in an optimal solution. This key distinction contributes dominantly to the performance difference. As discussed in Section III-B, Step 2 in the lateral guidance logic is designed for its simplicity, not optimality. For some other initial conditions, the lateral guidance logic can actually produce a trajectory much closer to the optimal one. Nonetheless we choose the current case to illustrate the possible difference.

Another noteworthy phenomenon in the optimal bank angle history in Fig. 9 is that the bank angle at the end is not zero. This means that the optimal trajectory is still turning at the end, which makes sense because for the same amount of heading change, smaller bank

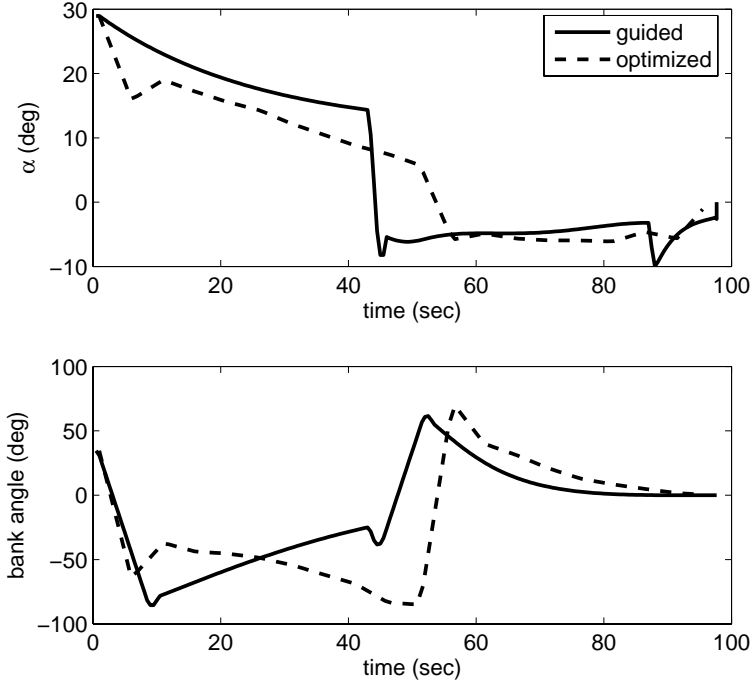


Figure 6: Angle of attack and bank angle for the vertical impact case

angle will be needed near the end where the velocity is lowest along the trajectory. Without using large bank earlier the trajectory is kept aloft, thus minimizing the velocity loss. But nonzero bank angle at the end also suggests that the vehicle's heading angle is not in steady state. Therefore the timing and the bank angle must match perfectly to achieve the specified final heading angle. Again this is something that requires heavy computation, and cannot be attained with simple logic.

The parameter adaptation laws (53) and (57) with $\kappa_1 = \kappa_2 = 4$ are responsible for the high accuracy in the final conditions of the impact angles in this case. Without the adaptation, the final conditions would have been $\gamma_f = -58.75$ deg and $\psi_f = 88.36$ deg, respectively. In Fig. 10 the variation of λ_1 is plotted. The execution of Step 2 of the lateral guidance logic (Eq. (30)) takes about 10 seconds at the beginning of the terminal phase. After that, Step 3 of the lateral guidance logic becomes active, and this is when the adaptation of λ_1 starts. The value of λ_1 stays nearly constant until Step 2 (and then

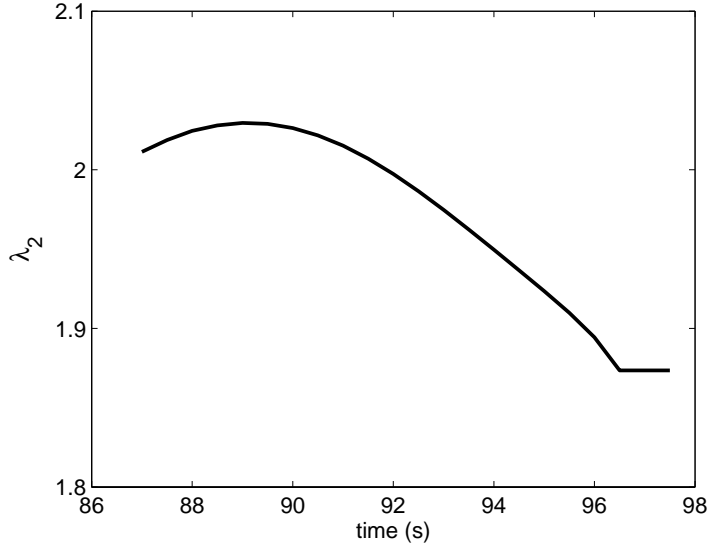


Figure 7: The adaptation history of λ_2 for the vertical impact case

Step 3) of the longitudinal guidance logic begins to take effect. The coupling effects of the longitudinal maneuvers cause the adaptation law (57) to sense the need for final adjustments in the heading in order to meet the constraint Eq. (64). The large variation of λ_1 in Fig. 10 underscores the difficulty of changing the heading of a hypervelocity vehicle, even for relatively small corrections. Figure 11 contains the adaptation history of λ_2 for this case, which is comparatively minor.

The remarkable possibility of achieving near optimality by the guidance logic proposed in the case of unconstrained final heading angle is even more evident in this example. For the same initial conditions as in Eq. (65), suppose that only constraint (63) is required, not Eq. (64). The lateral guidance law is just Eq. (10) with a constant $\lambda_1 = 3$ throughout the trajectory. The guided trajectory this time yields a final velocity of 1,030.7 m/s with $\gamma_f = -60.03$ deg and $s_f = 0.0004$ m. In contrast, the optimal trajectory without the final heading constraint Eq. (64) produces a final velocity of 1116.5 m/s. The performance difference between the two is significantly smaller in this case. Figure 12 illustrates the comparison of the angle of attack and bank angle histories. Except initially, the angle of attack profiles match quite well in about 2/3 of the flight. The bank angle histories, on the

other hand, are very close to each other throughout the trajectory.

VI. Conclusions

The need to guide a hypersonic lifting vehicle in terminal phase intended to impact a ground target with stringent specified impact direction arises from a recent technology development effort. We have found that an adaptive proportional-navigation guidance approach is effective to this problem and easy to implement. Our analysis establishes the theoretical attainment of the targeting conditions by the guided trajectories without relying on linearization or other simplifying assumptions. We provide closed-form conditions for the on-line selection of the initial values of the guidance parameters for satisfying the unique final impact angle requirements. For ensured high precision in the impact angle conditions, continuous closed-loop update of these parameters are necessary. For this purpose we further develop nonlinear parameter adaptation laws. The guidance logic developed is demonstrated to be accurate in 3 degrees-of-freedom simulations where the full nonlinear point-mass dynamics are included. It is interesting to note that in the absence of a final heading constraint, the trajectories under the proposed guidance logic behave in a similar fashion to optimal solutions that are generated off-line.

Acknowledgement

This work was supported in part by the USAF Contract F33615-01-C-3114.

References

- ¹ “Force Application and Launch from CONUS (FALCON)”, Broad Agency Announcement 03-35, DARPA, July 29, 2003, Arlington, VA.
- ² Cameron, J. D. M., “Explicit Guidance Equations for Maneuvering Re-entry Vehicles”, Proceedings of the IEEE Conference on Decision and Control, Vol. 1, New Orleans, LA., December 1977, pp. 670–678.
- ³ Page, J. A., and Rogers, R. O., “Guidance and Control of Maneuvering Reentry Vehicles”, Proceedings of the IEEE Conference on Decision and Control, Vol. 1, New Orleans, LA., December 1977, pp. 659–664.
- ⁴ Gracey, C., Cliff, E. M., Lutze, F. H., and Kelley, H. J., “Fixed-Trim Re-Entry Guidance Analysis”, *Journal of Guidance, Control, and Dynamics*, Vol. 5, No. 6, 1982, pp. 558–563.
- ⁵ Song, T. L., Shin, S. J., and Cho, H., “Impact Angle Control for Planar Engagements”, *IEEE Transactions on Aerospace and Electronic Systems*, Vol. 35, No. 4, 1999, pp. 1439–1444
- ⁶ Kim, B. S., Lee, J. G., and Han, H. S., “Biased PNG Law for Impact with Angular Constraint” *IEEE Transactions on Aerospace and Electronic Systems*, Vol. 34, No. 1, 1998, pp. 277–288
- ⁷ Lu, P., “Intercept of Nonmoving Targets at Arbitrary Time-Varying Velocity”, *Journal of Guidance, Control, and Dynamics*, Vol. 21, No. 1, 1998, pp. 176–178.
- ⁸ Vinh, N. X., *Flight Mechanics of High-Performance Aircraft*, Cambridge University Press, Cambridge, UK, 1993, pp. 22–25.
- ⁹ Vidyasagar, M., *Nonlinear Systems Analysis*, Prentice-Hall, Englewood Cliff, NJ, 1978, pp. 147–171.

¹⁰ *U. S. Standard Atmosphere, 1976*, NOAA, NASA, USAF, Washington, D. C., 1976.

¹¹ Ho, Y. C., Bryson, A. E., and Baron, S., “Differential Games and Optimal Pursuit-Evasion Strategies”, *IEEE Transactions on Automatic Control*, Vol. AC-10, No. 4, 1965, pp. 385–389.

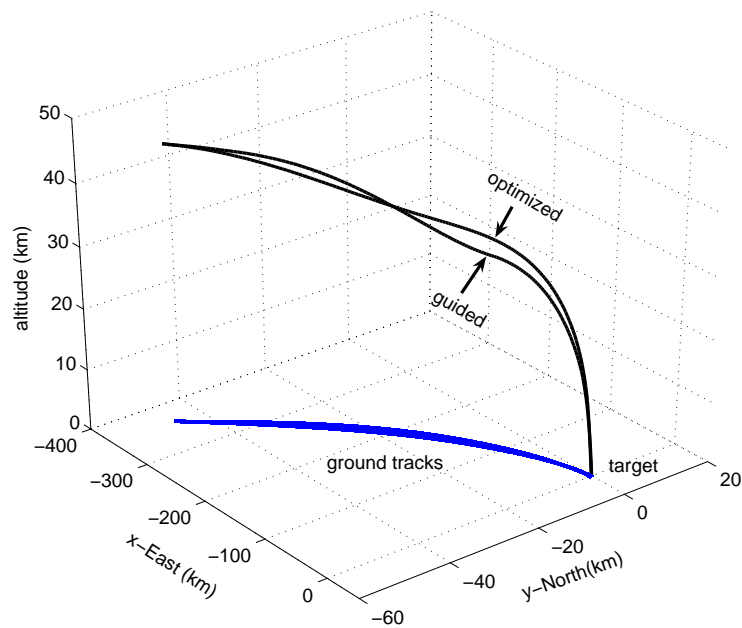


Figure 8: Three-dimensional trajectories for the non-vertical impact case

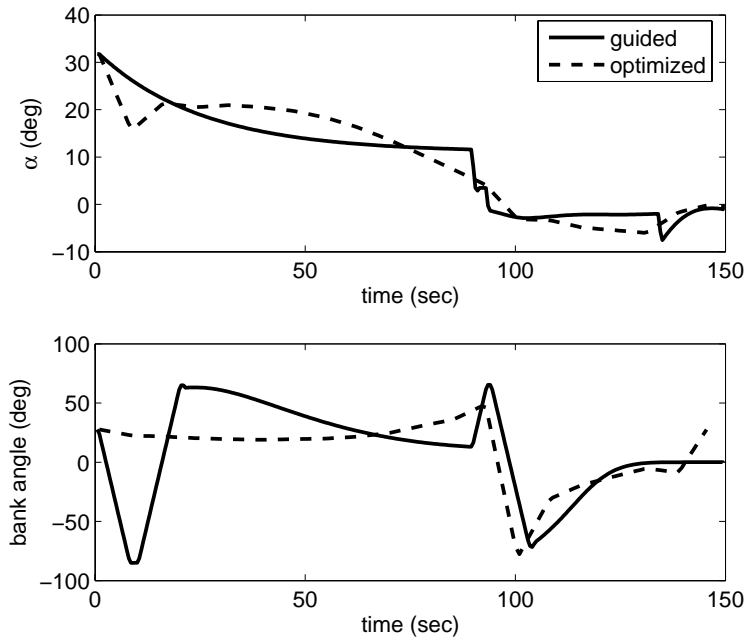


Figure 9: Angle of attack and bank angle for the non-vertical impact case with final heading constraint

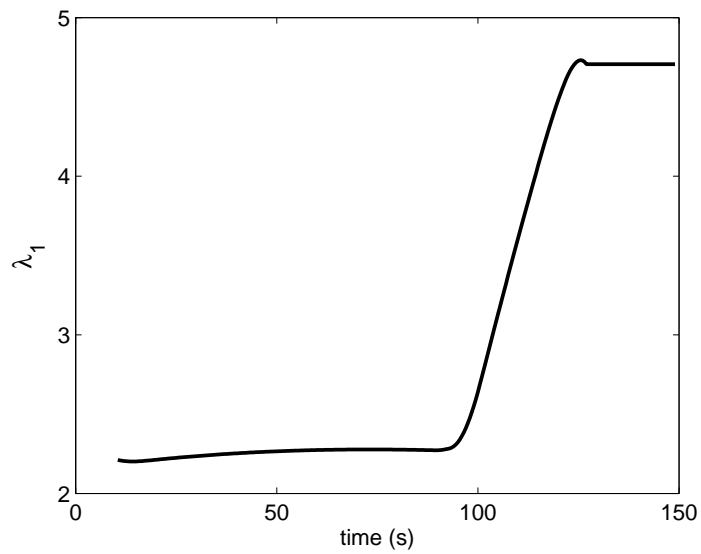


Figure 10: The adaptation history of λ_1 for the non-vertical impact case with final heading angle constraint

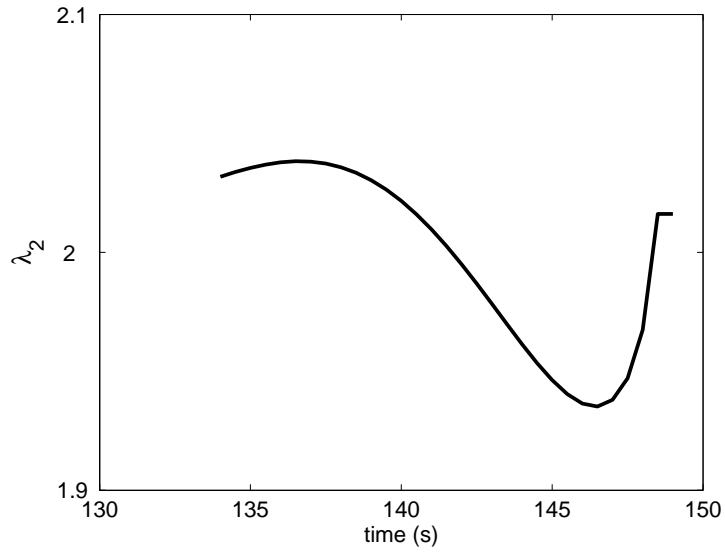


Figure 11: The adaptation history of λ_2 for the non-vertical impact case

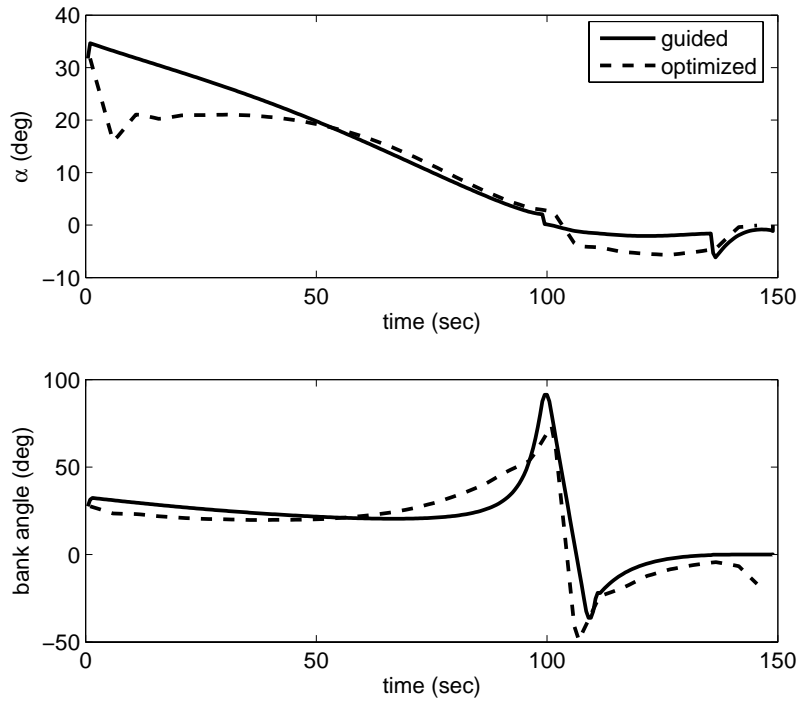


Figure 12: Angle of attack and bank angle for the non-vertical impact case without the final heading constraint